

Precision Early Universe Cosmology from Stochastic Gravitational Waves

David Brzemin^a, Anson Hook^a, and Gustavo Marques-Tavares^a

^aMaryland Center for Fundamental Physics, University of Maryland, College Park, MD 20742

E-mail: dbrzemin@umd.edu, hook@umd.edu, gusmt@umd.edu

ABSTRACT: The causal tail of stochastic gravitational waves can be used to probe the energy density in free streaming relativistic species as well as measure $g_*(T)$ and beta functions $\beta(T)$ as a function of temperature. In the event of the discovery of loud stochastic gravitational waves, we demonstrate that LISA can measure the free streaming fraction of the universe down to the 10^{-3} level, 100 times more sensitive than current constraints. Additionally, it would be sensitive to $\mathcal{O}(1)$ deviations of g_* and the QCD β function from their Standard Model value at temperatures $\sim 10^5$ GeV. In this case, many motivated models such as split SUSY and other solutions to the Electroweak Hierarchy problem would be tested. Future detectors, such as DECIGO, would be 100 times more sensitive than LISA to these effects and be capable of testing other motivated scenarios such as WIMPs and axions. The amazing prospect of using precision gravitational wave measurements to test such well motivated theories provides a benchmark to aim for when developing a precise understanding of the gravitational wave spectrum both experimentally and theoretically.

Contents

1	Introduction	1
2	Sensitivity of future experiments to the causal tail of stochastic GWs	4
2.1	SNR and Fisher matrix	5
2.2	Equation of state	7
2.3	Free-streaming fraction	10
3	Implications for well motivated models	12
3.1	$\sigma_w \lesssim 10^{-3}$	13
3.2	$\sigma_w \lesssim 10^{-5}$	14
3.3	$\sigma_{f_{FS}} \lesssim 10^{-2}$	15
4	Massive free streaming particles	15
4.1	Derivation of the damping	16
4.2	Numerical results	18
5	Conclusion	19
A	Calculation of $w(T)$	20

1 Introduction

With the discovery of gravitational waves by LIGO, we have added a new window with which to view the universe [1]. Due to its extremely weak coupling, gravitational waves (GWs) provide an almost unperturbed view of the universe. As such, they represent a unique opportunity with which to learn about early universe cosmology. Additionally, many new gravitational wave detectors are expected to be built in the future, such as LISA [2], BBO [3], MAGIS [4] and DECIGO [5], which will enhance our ability to observe GWs by many orders of magnitude.

If observed, stochastic gravitational waves would be the gravitational equivalent of the Cosmic Microwave Background (CMB), and thus, much could be learned from their detection. Similar to the CMB, the first thing we would likely learn is the mechanism by which GWs were generated. In the case of the CMB, it was black body radiation, while for GWs there exist a vast number of possibilities for production mechanisms [6–26]. Aside from having many different possible sources, the theories that give rise to stochastic GWs are also well motivated [27–36]. As with the CMB, angular anisotropies would encode information about

primordial fluctuations and could be used to learn more about inflation [37]. For example, the lack of a correlation between stochastic GWs and the CMB could indicate the presence of an additional light particle present during inflation.

Famously, propagation effects also leave an imprint on a cosmic background. For the CMB, this allowed a precise determination of the dark energy density and also gives sensitive to the matter power spectrum at lower redshift through lensing effects. In addition, future probes of the 21 cm absorption line can be used to determine other properties of the early universe. In the case of stochastic GWs, there are two main propagation effects that can change the GW spectrum coming from the equation of state of the universe ($w(T)$) and from relativistic free-streaming particles ($f_{FS}(T) = \rho_{FS}/\rho_{\text{total}}$). Both $w(T)$ and $f_{FS}(T)$, as well as changes to them, can be in principle observed from the frequency spectrum of a stochastic GW background [16, 17, 29, 30, 35, 37–54].

The expected sensitivity of 21 cm experiments is due to knowing that the CMB follows a blackbody spectrum ahead of time, so that deviations from this predicted spectrum can be attributed to propagation effects. In contrast, the stochastic GW spectrum is completely unknown. Even if observed, it will be a highly non-trivial task to make a prediction for what different parts of the spectrum should look like in the absence of propagation effects. As such, it would appear that propagation effects would be impossible to disentangle from the source generating the spectrum. However, there is an important case where we do know the shape of the spectrum ahead of time, the low frequency limit of causally produced GWs [38, 54, 55].

If the source producing GWs is only active for a short time period, this source is necessarily uncorrelated on distance scales longer than the time it took to produce the GWs (e.g. distances longer than the Hubble size are necessarily uncorrelated). This fact determines the shape of the GW spectrum at large wavelengths completely independent of the details of how the GW was generated. As an example, the low frequency tail of GWs generated by phase transitions is universal regardless of the details of the phase transition itself. In contrast, the low frequency tail of inflationary GWs is model dependent and cannot be predicted a priori. Thus, by studying the low frequency tail of stochastic GWs generated by a time localized source, one can learn about early universe dynamics through propagation effects on the GW spectrum.

In this paper, we study how sensitive future experiments, such as LISA and DECIGO, will be to propagation effects and provide well-motivated benchmark models to illustrate what can be achieved with varying levels of sensitivity. We find that in the event of a large stochastic GW background, LISA could measure $w(T)$ and f_{FS} with an accuracy of $\sim 10^{-3}$ over a temperature range of $10^4 - 10^6$ GeV. This demonstrates that LISA’s sensitivity to f_{FS} can be 10–100 times more sensitive than even CMB S4 experiments. Future experiments such as DECIGO can measure $w(T)$ and f_{FS} with an accuracy of 10^{-6} and extended sensitivity to an even higher temperature range of $10^4 - 10^8$ GeV.

In the case of a radiation dominated universe, being able to measure $w(T)$ at the $10^{-4} - 10^{-3}$ level is a complete game changer. While one might think that $w = 1/3$ at high temperatures, due to the scale anomaly $w(T) - 1/3 \sim \beta(T)/g_*(T)$ where β is a combina-

tion of Standard Model (SM) beta functions with the QCD beta function giving the largest contribution. For the SM, $w(T) - 1/3 \sim 5 \times 10^{-4}$. Thus LISA could, in principle, test the SM prediction that $w \neq 1/3$ in a radiation dominated universe.

Aside from the possible spectacular confirmation of a SM prediction, these measurements can test some of the most well motivated particle physics models related to the Electroweak Hierarchy problem [56, 57] and dark matter [58]. Dimensional analysis predicts that the physics responsible for the mass of the Higgs boson should be at the TeV scale. Solutions to this problem often require doubling the number of particles in the SM. At temperatures above the TeV scale, this would double g_* and/or β and hence change the predicted value of $w(T > \text{TeV})$ by $\mathcal{O}(10^{-4} - 10^{-3})$, something testable by LISA.

There is also strong reason to expect the mass of dark matter to be below the 100 TeV scale. If what is responsible for dark matter was ever in thermal contact with the SM, then modulo some mild assumptions, unitarity requires that the energy scale of dark matter be below 100 TeV [59]. A classic motivated example of such a dark matter particle is the famous weakly interacting massive particle (WIMP). WIMPs have a TeV scale mass whose precise value depends on their representation under $SU(2)$. In the early universe, at temperatures $T \gtrsim 100 \text{ TeV}$, dark matter would be in thermal equilibrium and change g_* by ~ 1 . WIMP dark matter would thus be guaranteed to change $w(T)$ by $\mathcal{O}(10^{-5})$. While LISA cannot reach this sensitivity, future detectors such as DECIGO could potentially test all thermal dark matter candidates.

Precision measurements of f_{FS} in the early universe are equally important. It is worth prefacing the discussion of f_{FS} by noting that we have no direct observations of the radiation domination epoch with $f_{FS} < 0.3$. Thus even a negative measurement would indicate a phase of the universe that we have never observationally seen before. One important benchmark is $f_{FS} \sim 10^{-2}$, which is the value of a single new degree of freedom that was in thermal equilibrium but has since left equilibrium. In many motivated models, such as the QCD axion [60–63], there is at least one new particle of this sort and reaching sensitivities of the order of $\mathcal{O}(10^{-2})$ would constitute an important test of these theories. Additionally, as GWs are themselves free streaming, one could even measure the backreaction of GWs on themselves if the stochastic GW signal was loud enough. Like the neutrinos, new free streaming particles beyond the Standard Model may become non-relativistic after going out of equilibrium with the SM bath. We also explore how this behavior changes the effect of free streaming particles on GWs.

In Sec. 2, we discuss the sensitivity of GW detectors to $w(T)$ and $f_{FS}(T)$. In Sec. 3, we discuss the impact of these measurements on well motivated models. In Sec. 4, we discuss in more detail how massive free streaming particles change the GW spectrum. We finish with concluding remarks in Sec. 5

2 Sensitivity of future experiments to the causal tail of stochastic GWs

In this section we discuss the sensitivity of GW experiments to the low frequency tail of causally produced GWs. It is well known that the low frequency tail of any time localized, causally produced GW has a fixed form regardless of how it was produced [55]. The fixed form of this low frequency tail depends on details such as the equation of state $w(T)$ in the era following the production of the GW [38, 54]. Different values of $w(T)$ give the function form for the gravitational wave power spectrum

$$\Omega_{GW}(k) \propto k^{3-2\left(\frac{1-3w}{1+3w}\right)}, \quad (2.1)$$

where w is the equation of state when the mode with wave-number k entered the horizon. Aside from the equation of state, the low frequency tail is also sensitive to the free-streaming fraction

$$f_{FS}(T) = \frac{\rho_{FS}(T)}{\rho_{\text{total}}(T)}. \quad (2.2)$$

Weinberg first showed that free streaming particles can dampen inflationary gravitational waves [64] and similar effects were shown to be present for non-inflationary GWs [38]. As a GW travels, it imparts a quadrupole moment on any ambient free streaming particles that subsequently backreacts and suppresses the GW in much the same way that a dielectric suppresses electric fields. Assuming radiation domination and relativistic free-streaming particles, the dependence is of the form

$$\Omega_{GW}(k) \propto k^{3+\frac{16}{5}f_{FS}} \quad (2.3)$$

in the limit where $f_{FS} \ll 1$ [38]. The explicit form for arbitrary f_{FS} , including the case where $f_{FS} \gtrsim 5/32$ when Ω_{GW} develops an oscillatory pattern, must be calculated numerically (see Eq. 2.20 for its approximate analytical form). We can see from Eq. 2.1 the famous fact that in a radiation dominated era ($w = 1/3$) with no relativistic free streaming particles, the spectrum is predicted to scale exactly as k^3 . Any deviation from k^3 scaling would be evidence of free streaming particles or that $w \neq 1/3$.

A transfer function can be used to take into account the effects of w or f_{FS} on the GW spectrum. Given a GW spectrum that was calculated/numerically simulated in a radiation dominated universe ($\Omega_{GW}^0(k)$), we can take into account $w \neq 1/3$ and/or $f_{FS} \neq 0$ using

$$\Omega_{GW}(k, \theta) = \Omega_{GW}^0(c(\theta)k) F(c(\theta)k, \theta), \quad (2.4)$$

where $\theta = w$ or f_{FS} , and $c(\theta)$ is a re-scaling of frequencies that arises due to the change in the redshift at which the GWs were produced (since the temperature will evolve differently as a function of redshift for different $w(T)$)¹. $\Omega_{GW}^0(k)$ is the spectrum for $w = 1/3$ and $f_{FS} = 0$,

¹This is equivalent to a rescaling of the frequency and does not affect the shape of the spectrum. As the shape of the spectrum will be the main focus of our analysis, and because a shift in the frequency scales is

while $F(k, \theta)$ is a transfer function that encapsulates how the spectrum depends on these additional parameters and will be specified in their respective subsections. When estimating the sensitivity of GW detectors to θ , we need to specify $\Omega_{GW}^0(k)$.

We will take $\Omega_{GW}^0(k)$ to be the gravitational wave spectrum coming from the sound waves of a phase transition, but the results of this paper will apply for any causal source of gravitational waves. For simplicity, we will use an analytical approximation of numerical results [65]²

$$h^2 \Omega_{GW}^0 = 1.19 \times 10^{-6} \left(\frac{H_{PT}}{\beta} \right) \left(\frac{\kappa_v \alpha}{1 + \alpha} \right)^2 \left(\frac{100}{g_\star} \right)^{1/3} \left(\frac{f}{f_\star} \right)^3 \left(\frac{7}{4 + 3(f/f_\star)^2} \right)^{7/2}, \quad (2.5)$$

$$f_\star = 8.9 \times 10^{-3} \text{ mHz} \frac{1}{v_w} \left(\frac{\beta}{H_{PT}} \right) \left(\frac{T_{PT}}{100 \text{ GeV}} \right) \left(\frac{g_\star}{100} \right)^{1/6}, \quad (2.6)$$

where f_\star is the peak frequency of the spectrum, T_{PT} (H_{PT}) is the temperature (Hubble scale) at which the phase transition took place, $\alpha = \rho_{PT}/\rho_{\text{total}}$ is the ratio of the energy released by the PT to the total energy density, the time scale of the transition is $1/\beta$, and $\kappa_v = \alpha/(0.73 + 0.083\sqrt{\alpha} + \alpha)$ is the fraction of the latent heat which gets converted into the bulk motion of the fluid. In the last expression, we are also assuming a large wall velocity $v_w \sim 1$.

2.1 SNR and Fisher matrix

The visibility of a stochastic GW background is typically encapsulated by its signal-to-noise ratio (SNR). In a detector like LIGO, with two (or more) independent interferometers, a stochastic GW signal is searched for by comparing the power in two different GW detectors, 1 and 2. The SNR is [68–70]

$$\text{SNR}^2 = 2T \int_{-\infty}^{\infty} \frac{df}{2} \frac{|U(f)|^2}{|U(f)|^2 + W(f)}, \quad (2.7)$$

where

$$U(f) = C_{12}(f), \quad (2.8)$$

$$W(f) = C_{11}(f)C_{22}(f) + C_{11}(f)N_2(f) + C_{22}(f)N_1(f) + N_1(f)N_2(f). \quad (2.9)$$

also achieved by rescaling the unknown temperature of the PT, we will neglect this rescaling of frequency from now on.

²The dependence of the spectral shape of the sub-horizon modes on the physics of the PT is still an active topic of investigation, for some recent discussion see e.g. [16, 66, 67]

The functions C and N are defined as

$$C_{IJ}(f; t, t) = \int \frac{d\Omega}{4\pi} S_h(f) \mathcal{F}_{IJ}(f, \Omega; t, t), \quad (2.10)$$

$$\langle \tilde{n}_I^*(f) \tilde{n}_J(f') \rangle = \frac{1}{2} \delta_{IJ} \delta(f - f') N_I(f), \quad (2.11)$$

$$\langle \tilde{h}_A^*(f, \Omega) \tilde{h}_{A'}(f', \Omega') \rangle = \frac{1}{2} \delta(f - f') \frac{\delta^2(\Omega, \Omega')}{4\pi} \delta_{AA'} S_h(|f|, \Omega), \quad (2.12)$$

where the indices I, J represent the different detectors used to capture the signal, and \mathcal{F}_{IJ} is the antenna pattern function [70], which characterizes the overlap in the detectors response to the signal. \tilde{n} is the noise while \tilde{h} is the GW signal. Indices A, A' represent polarization of the GW signal, f is the frequency of the GW while Ω is the direction it is coming from. For simplicity we assume that the signal is isotropic so that

$$\Omega_{GW}(f) = \frac{8\pi G}{3H_0^2} \frac{d\rho_{GW}}{d\log f} = \frac{4\pi}{3} \frac{f^3 S_h(f)}{H_0^2}. \quad (2.13)$$

Here H_0 is the value of the Hubble parameter today. As an additional simplification, we also take the various overlap factors between detectors to be identical, $\mathcal{F}_{12} = \mathcal{F}_{11} = \mathcal{F}_{22}$, and the noise of the two detectors to be the same, $N_1 = N_2$. As a result the SNR simplifies to

$$\text{SNR}^2 = T \int df \frac{\Omega_{GW}^2}{2\Omega_{GW}^2 + 2\Omega_{GW}\Omega_{\text{noise}} + \Omega_{\text{noise}}^2}, \quad (2.14)$$

where T is the runtime of the experiment and Ω_{noise} is the noise power spectrum (normalized to the critical density as in Eq. 2.13). While for future space-base missions this approach is not exactly justified, it recovers the usual SNR expression in the small signal limit (see e.g. [47]) (which to our knowledge is the only case that has been widely studied), and at least incorporates some of the important effects of the large signal limit.

We can obtain an intuitive understanding of Eq. 2.14 by using the fact that the signal is a measurement of the cross correlation between detectors, schematically

$$S = \mu = \langle (h + n_1)(h + n_2) \rangle \propto \Omega_{GW}. \quad (2.15)$$

Meanwhile, the noise is schematically

$$\begin{aligned} N^2 &= \Sigma = \langle (h + n_1)^2 (h + n_2)^2 \rangle - \langle (h + n_1)(h + n_2) \rangle^2 \\ &\propto 2\Omega_{GW}^2 + 2\Omega_{GW}\Omega_{\text{noise}} + \Omega_{\text{noise}}^2, \end{aligned} \quad (2.16)$$

where we have taken the usual approximation that the GW signal is approximately Gaussian. Taking $\text{SNR} = S/N$ for each frequency bin and summing in quadrature over all of the frequency bins gives Eq. 2.14.³

³These expressions will also play a role in forecasting the sensitivity of future space based experiments,

In this article, we will be usually working in the optimistic limit where the signal is large. As can be seen in Eq. 2.14, under this approximation the magnitude of the noise is less important than the runtime and the frequency range under consideration. Thus, for us, the main difference between experiments when it comes to measuring $w(T)$ or $f_{FS}(T)$ is the difference in frequency ranges that they are sensitive to.

To estimate the sensitivity of an experiment to $w(T)$ or $f_{FS}(T)$, we will use the Fisher information matrix (for recent studies forecasting LISA sensitivity to spectral information of GW signals see e.g. [71, 72]), and assume that we will be able to subtract contamination from astrophysical foregrounds. The Fisher matrix is useful because it determines the optimal sensitivity of any unbiased estimator. Assuming gaussian distributions, the Fisher information matrix can be found from the covariance matrix Σ and mean μ using

$$F_{\alpha\beta} = \frac{\partial\mu}{\partial\theta_\alpha} \Sigma^{-1} \frac{\partial\mu}{\partial\theta_\beta} + \frac{1}{2} \text{Tr} \left(\Sigma^{-1} \frac{\partial\Sigma}{\partial\theta_\alpha} \Sigma^{-1} \frac{\partial\Sigma}{\partial\theta_\beta} \right) \quad (2.17)$$

$$= T \int df \frac{\partial\Omega_{GW}}{\partial\theta_\alpha} \frac{\partial\Omega_{GW}}{\partial\theta_\beta} \frac{4\Omega_{GW}^2 + 2\Omega_{GW}\Omega_{\text{noise}} + \Omega_{\text{noise}}^2}{(2\Omega_{GW}^2 + 2\Omega_{GW}\Omega_{\text{noise}} + \Omega_{\text{noise}}^2)^2}, \quad (2.18)$$

where θ_α are the parameters describing the GW spectrum. For example, if we let w be quantity of interest, then we can replace $\theta_{\alpha,\beta} \rightarrow w$ and the Fisher matrix $F = 1/\sigma_w^2$ describes the variance in how well an experiment could measure w . In later subsections, we will utilize Eq. 2.17 to calculate the sensitivity of LISA and DECIGO to the equation of state and f_{FS} . For LISA we take Ω_{noise} from program PTPlot [16] and for DECIGO we take Ω_{noise} from Ref. [73]. In both cases, we take the runtime of the experiment to be $T = 10^8$ seconds.

2.2 Equation of state

When studying the sensitivity of experiments to the equation of state, we first need to fully specify the GW spectrum, namely we need to determine $F(k, w)$ shown in Eq. 2.4 assuming no relativistic free streaming species ($f_{FS} = 0$). In the limit that the phase transition occurred very rapidly, $\beta/H_{PT} \gtrsim 1$, and for wavelengths that are larger than the spatial correlations of the source, this function can be analytically shown to be [38]

$$F(k, \theta = w) = \frac{|j_{\frac{1-3w}{1+3w}}(k\tau_{PT})|^2 + |y_{\frac{1-3w}{1+3w}}(k\tau_{PT})|^2}{|j_0(k\tau_{PT})|^2 + |y_0(k\tau_{PT})|^2}, \quad (2.19)$$

where τ_{PT} is the conformal time when the phase transition occurred and j_n and y_n are the spherical Bessel functions. For simplicity, we will take this to hold even when $\beta/H_{PT} \sim 1$.

With the full GW spectrum in hand, we can use Eq. 2.17 to find the sensitivity of any given experiment to the equation of state of the universe. For simplicity we will express our sensitivity to $\delta w = w - 1/3$ in the form of the variance σ_w . In principle, the phase transition

even though, as mentioned earlier, they are technically only valid for a LIGO like setup. One can show that they lead to expressions for the fisher matrix that match the literature [47] both in the small signal limit and in the signal much larger than noise limit, and thus will be used in our analysis.

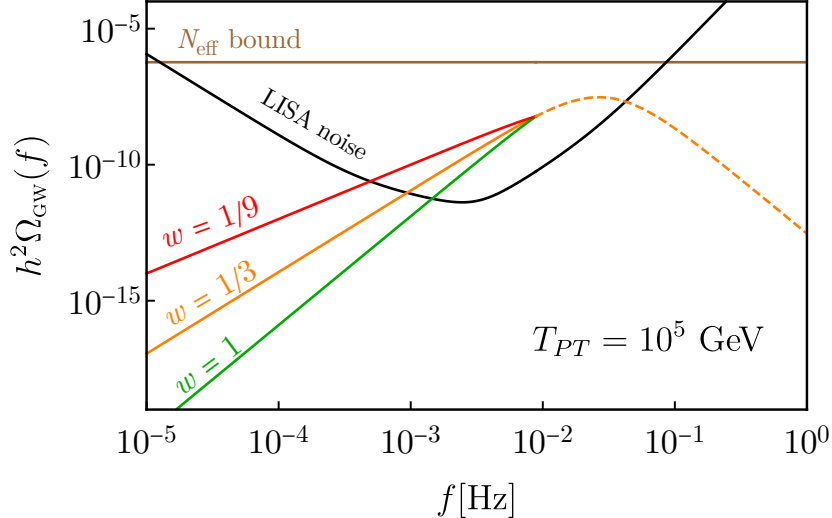


Figure 1. A graphical representation of how the gravitational wave spectrum changes for various $w(T)$ compared to the LISA sensitivity curve assuming a runtime of 10^8 s. For simplicity we are only showing how the shape changes and neglecting the rescaling of frequencies due to differing expansion histories. The dashed line indicates modes that were sub-horizon at the time the phase transition took place and their shape is unaffected by the change in expansion history. The solid lines indicate modes that were super-horizon at the time when the phase transition took place and have their shape distorted by the different expansion history.

parameters $(\alpha, \beta, T_{PT}, \dots)$ can all be determined from the peak of the distribution and thus we will take them to be fixed while studying the sensitivity to δw .⁴ In order to show how σ_w depends on various phase transition parameters, we first fix all parameters except for T_{PT} and a single other parameter and show how σ_w varies as a function of a T_{PT} for a few values of the other parameter. Motivated by one of the louder phase transition models from Ref. [44], we will take $\alpha = 1$, $\beta = 3$ and $v_w = 1$ unless otherwise stated.

To show visually how $w(T)$ affects the GW spectrum, in Fig. 1 we show how the GW spectrum changes as one changes $w(T)$. We will be interested in small changes around $w = 1/3$. Due to the similar scaling of the background noise and the signal, the signal remains above background for a large range of frequencies, leading to sensitivity over a wide range of frequencies (and thus a wide range of temperatures in the early universe). We will first study the sensitivity σ_w to constant deviations in the equation of state before studying the sensitivity to frequency/temperature dependent changes to the equation of state.

We first show how σ_w depends on α in Fig. 2. Varying α changes the amplitude of the signal. As can be seen from the SNR (Eq. 2.14) and the Fisher matrix (Eq. 2.17), the magnitude of the signal is not particularly important if the signal is larger than the background. This can be seen explicitly in Fig. 2 for the DECIGO sensitivity (for LISA the signal is only above the noise for a narrow range of parameters). For smaller T_{PT} , the

⁴As discussed earlier, we are also ignoring the shift in frequencies due to the difference in expansion history, which can in principle be reabsorbed by changing the phase transition parameters.

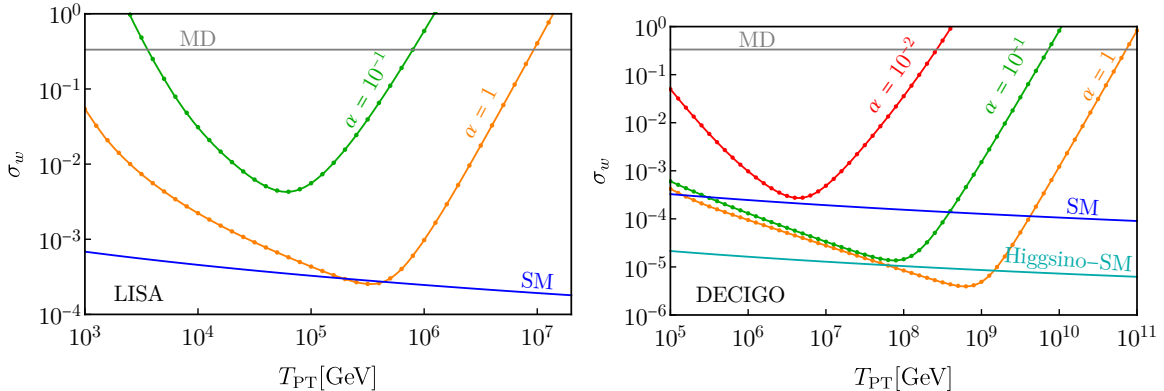


Figure 2. The projected sensitivity, calculated using the Fisher matrix, of LISA (left) and DECIGO (right) to a constant equation of state near $w = 1/3$ as a function of the temperature at which the phase transition occurred for various α . α controls the amplitude of a GW. For reference we show matter domination ($\delta w = -1/3$) as well as the SM and SM plus doublet dark matter predictions for δw versus temperature.

sensitivity is the same for $\alpha = 1$ and 0.1 . At higher T_{PT} , eventually the signal falls below the background and larger α results in better sensitivity. For $\alpha = 0.01$, background is important for all temperatures and thus the sensitivity is always worse than larger values of α .

Next, we show how σ_w depends on β in Fig. 3. Effectively, β is a measurement of how sub-horizon the physics that generates the GWs is. As such, while it has an impact on the peak of the spectrum, it does not have a large effect on the low frequency tail that we are interested in. The main effect of β is thus very similar to α , where it just changes the amplitude of the low frequency tail. As such, the qualitative behavior is quite similar. For the DECIGO sensitivity in Fig. 3, one sees that at low T_{PT} where the signal is much larger than noise, σ_w is insensitive to β , while at for high T_{PT} , σ_w is larger for smaller amplitudes (larger β).

In the previous two examples, we assumed that δw was temperature independent. One of the most exciting prospects would be if it is possible to measure $w(T)$ as a function of temperature. Assuming radiation domination from the temperature of T_{PT} to matter-radiation equality gives a one-to-one mapping between the measured frequency dependence and the desired temperature dependence (ignoring the small correction due to $\delta w \neq 1/3$ which can be easily included). As such, we separated frequency space into bins logarithmically spaced from $f/3$ to f . For each bin, we obtain the sensitivity to σ_w using Eq. 2.17 limiting the integration to be only over the corresponding frequency bin. The expected sensitivity for such analysis is shown in Fig. 4. From this we see the remarkable result that in the advent of a loud GW signal generated at large temperatures, a precise measurement of $w(T)$ can be made over a large range of temperatures.

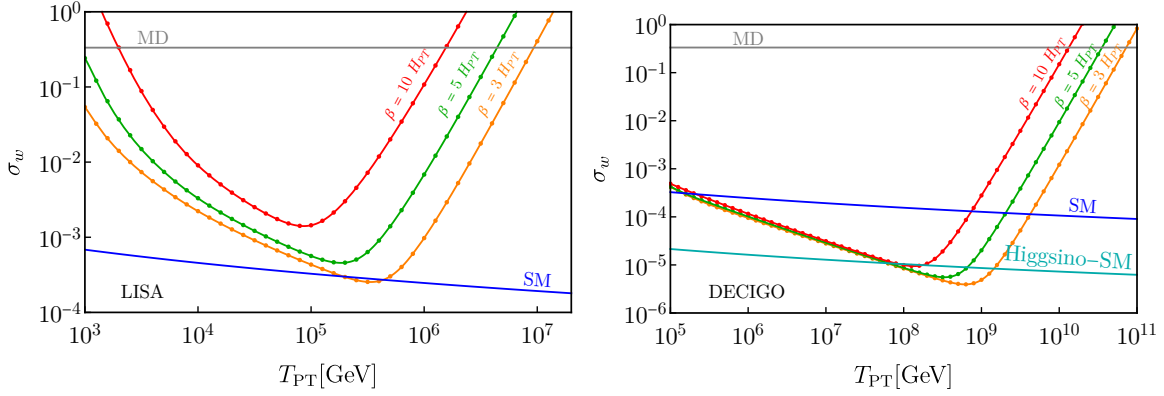


Figure 3. The projected sensitivity, calculated using the Fisher matrix, of LISA (left) and DECIGO (right) to a constant equation of state near $w = 1/3$ as a function of the temperature at which the phase transition occurred for various β . β controls the duration of the phase transition generating the GW. For reference we show matter domination ($\delta w = -1/3$) as well as the SM and SM plus doublet dark matter predictions for δw versus temperature.

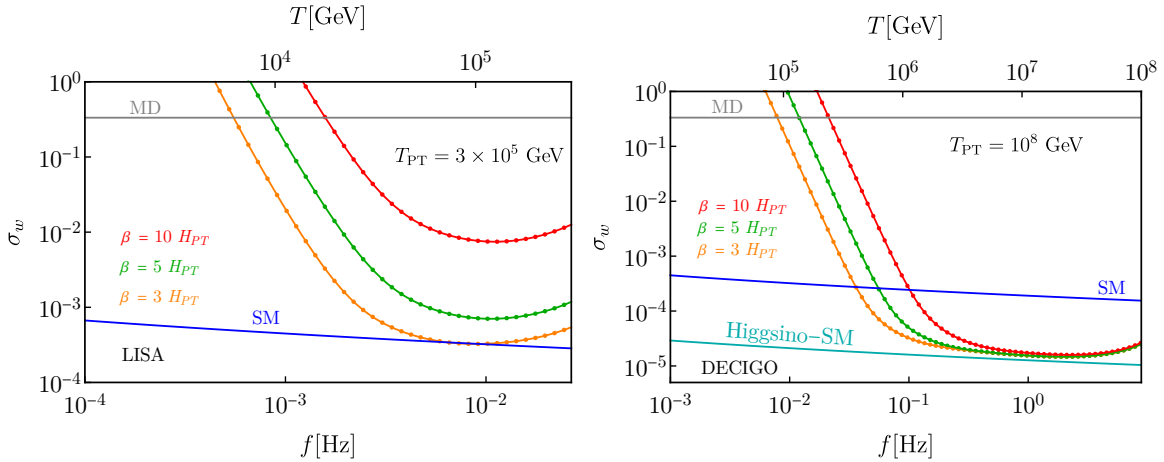


Figure 4. The projected sensitivity, calculated using the Fisher matrix, of LISA (left) and DECIGO (right) to the equation of state near $w = 1/3$ as a function of frequency for various T_{PT} . The sensitivity was obtained by binning the data logarithmically between a frequency f_0 and $f_0/3$.

2.3 Free-streaming fraction

The small free-streaming fraction limit and the small δw limit are similar in that, in both cases, the main observable effect is the change in the slope away from the k^3 scaling. As such, the results of the previous sub-section can be applied to non-zero f_{FS} by using the substitution $\sigma_w \rightarrow 16 \sigma_{f_{FS}}/15$ to obtain the sensitivity to free-streaming particles. If the free-streaming fraction $f_{FS} \lesssim 10^{-3}$, then at that point there is necessarily “background” coming from the SM predicting $\delta w \sim 10^{-3}$. In the small δw and f_{FS} limit, the similarity of these two signals leads to the unfortunate degeneracy that GW detectors are only sensitive to the

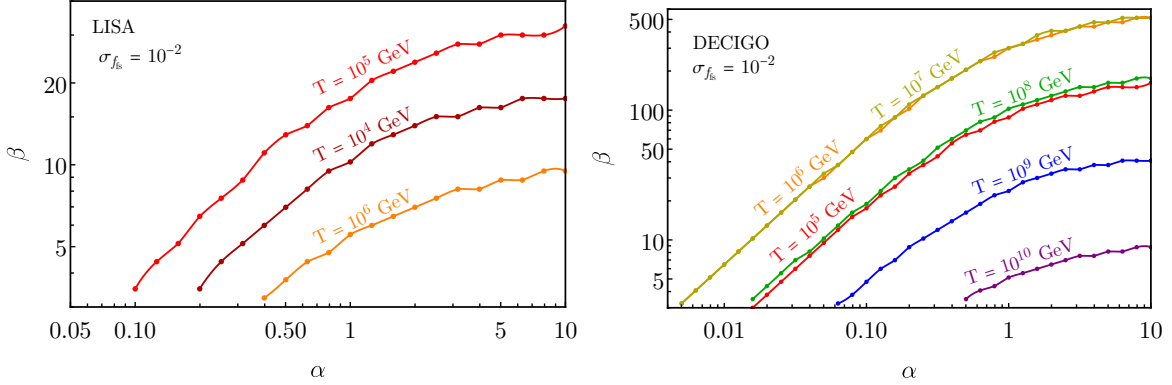


Figure 5. The regions of phase transition parameter space for which the well motivated value of $f_{FS} \sim 10^{-2}$ can be reached at LISA (left) and DECIGO (right). For a given value of T_{PT} , as long as the phase transition parameters α and β are to the right of the line, then a sensitivity of $f_{FS} \sim 10^{-2}$ can be obtained.

linear combination $\delta w + 16\sigma_{f_{FS}}/15$.

As we will see in Sec. 3, there is a well motivated benchmark of $f_{FS} \sim 10^{-2}$. Given this a well defined benchmark target, we will characterize for what values of the phase transition parameters this benchmark sensitivity can be achieved assuming that $\delta\omega = 0$. In Fig. 5, we show contours of fixed phase transition temperature T_{PT} versus the phase transition parameters α and β . For a given T_{PT} , if the phase transition parameters are to the right of the line, then a sensitivity of $f_{FS} \sim 10^{-2}$ can be achieved.

Aside from the small free streaming fraction limit, there is a unique behavior of free-streaming particles that manifests itself for large free streaming fractions. When the free streaming fraction is large, $f_{FS} > 5/32$, it induces oscillations in the GW spectrum. The precise form of the transfer function has to be computed numerically by solving an integro-differential equation (see Sec. 4), but for small frequencies it is well approximated by [38]

$$F(k, f_{FS} > 5/32) \propto k^{-1} \left[1 + C \sin \left(\log(kT_{PT}) \sqrt{\frac{32}{5} f_{FS} - 1 + \delta} \right) \right], \quad (2.20)$$

where C and δ are k independent functions of f_{FS} .

We now determine how accurately one can measure f_{FS} in the large f_{FS} limit. The signal of large f_{FS} comes in the form of oscillations on top of a k^{-4} fall off. The amplitude, phase and periodicity of the oscillation informs one about the value of f_{FS} . To get an understanding of LISA's sensitivity to f_{FS} in the large frequency limit, we consider the example $f_{FS} = 0.4$. Fixing f_{FS} to this value, we obtain the maximal sensitivity to f_{FS} using the Fisher analysis shown in Eq. 2.17. As before, we will take $\alpha = 1$, $\beta = 3$ and $v_w = 1$. The spectrum is shown visually in Fig. 6. Using Eq. 2.17, we find that a sensitivity of $\sigma_{f_{FS}} \sim 1.1 \times 10^{-3}$ can be reached.

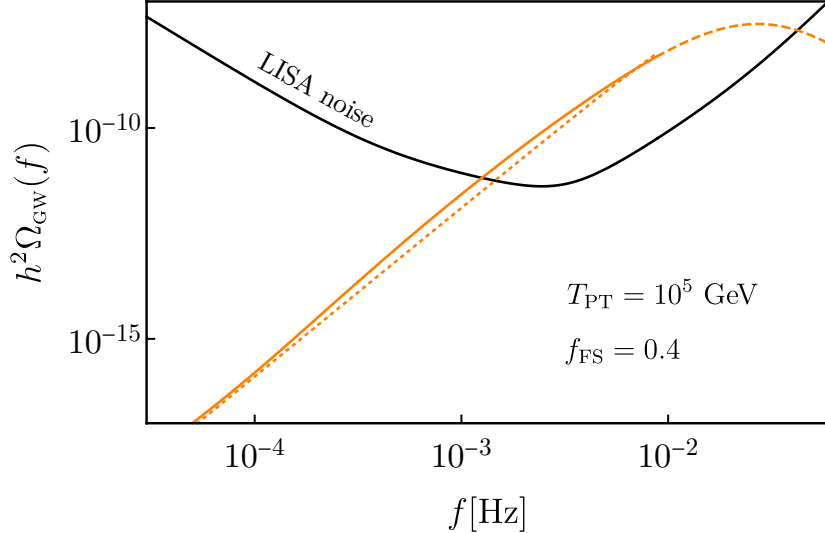


Figure 6. $\Omega_{GW}(f)$ versus frequency for a free-streaming fraction of $f_{FS} = 0.4$. The dashed line indicates the sub-horizon modes, the solid line are the super-horizon modes, and the dotted line is the f^4 fall off on top of which oscillations occur. The small oscillations are what allows one to distinguish between various large values of f_{FS} . For this particular example, a sensitivity of $\sigma_{f_{FS}} = 1.1 \times 10^{-3}$ can be obtained.

3 Implications for well motivated models

When making precision measurements of δw and f_{FS} , there are several benchmark points that are of great interest. For δw , the first benchmark is at $\delta w \sim 10^{-3}$ (achievable at LISA) while the second benchmark is $\delta w \sim 10^{-5}$ (achievable at DECIGO). For f_{FS} the benchmark value is $f_{FS} \sim 10^{-2}$ (achievable at LISA).

The reason why there are any benchmarks at all for δw , is because, as reviewed in the Appendix, for the SM in a radiation dominated universe

$$T_\mu^\mu = \rho - 3p, \quad \delta w(T = 10^5 \text{ GeV}) = \frac{T_\mu^\mu}{3\rho} \approx -3 \times 10^{-4} \left(\frac{100}{g_\star} \right) \left(\frac{\beta_{QCD}}{\beta_{QCD}^{SM}} \right). \quad (3.1)$$

The dependence of δw on the total number of degrees of freedom in the universe is what makes measuring δw so appealing. Many motivated models predict a doubling of the SM β functions and/or the number of degrees of freedom, resulting in a change in δw of $\sim 10^{-3}$, giving the benchmark. Meanwhile, if the SM is augmented by a single degree of freedom, δw changes by around 10^{-5} , giving the second benchmark. A simple well motivated example which has this feature is the famous WIMP dark matter candidate.

A measurement of f_{FS} to the order of 10^{-2} is important because that is the contribution one gets from a single new particle that freezes-out while relativistic, like the neutrinos do in the SM. Aside from the fact that it happens in the SM, there is good reason to expect that something similar could occur in the early universe as well. As an example, in many axion

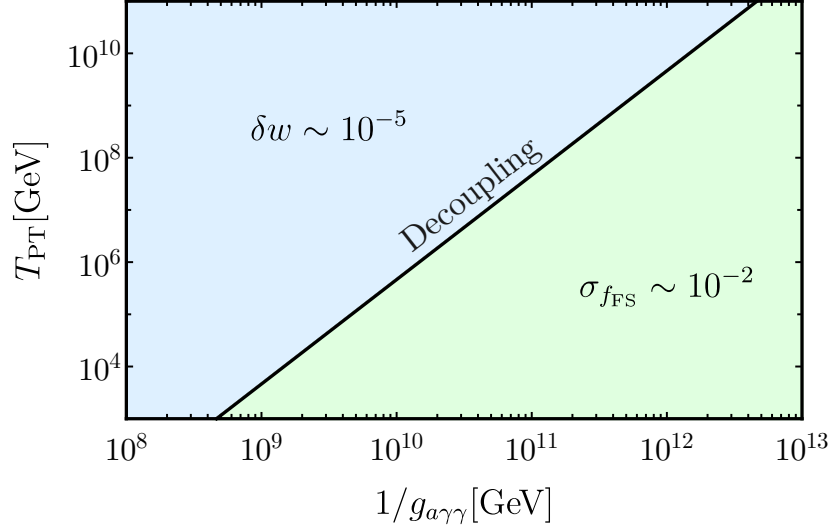


Figure 7. The region of axion parameter space that can be probed as a deviation from the equation of state or as a free streaming fraction. The black line, $T_{dec}(g_{a\gamma\gamma})$, gives the decoupling temperature of the axion as a function of the coupling to photons. In the blue region, axions in equilibrium with the SM predict $\delta w \sim 10^{-5}$ while in the green region, free streaming axions predict $f_{FS} \sim 10^{-2}$ so long as the reheating temperature, T_{RH} , satisfies $T_{RH} > T_{dec}(g_{a\gamma\gamma})$.

models, axions are in thermal equilibrium with the SM before freezing out. After freezing out, they become free-streaming particles and lead to $f_{FS} \sim 10^{-2}$.

As one particularly well motivated models for both δw and f_{FS} are axions, we show how different regions of axion parameter space can be probed with gravitational waves in Fig. 7. The black line is $T_{dec}(g_{a\gamma\gamma})$ and gives the decoupling temperature of the axions from the thermal bath as a function of the axion coupling to photons (assuming this is the largest coupling). The region of parameter space in blue predicts $\delta w \sim 10^{-5}$. Meanwhile, the region of parameter space in green predicts $f_{FS} \sim 10^{-2}$ as long as the reheating temperature obeys $T_{RH} > T_{dec}(g_{a\gamma\gamma})$.

Finally it is worth noting, that a non-zero measurement of δw or f_{FS} can very easily prevent a clean measurement of the other. So while it would be extremely exciting to measure one or the other non-zero, it is unlikely that everything mentioned in this section can be realized simultaneously.

3.1 $\sigma_w \lesssim 10^{-3}$

The strongest motivation for TeV scale physics lies within the electroweak hierarchy problem. Many solutions to this problem involve a large number of degrees of freedom. Perhaps the most famous of these solutions is supersymmetry (SUSY), for a review see Ref. [74]. Supersymmetry doubles the number of degrees of freedom and predicts

$$\delta w(T = 10^5 \text{ GeV}) = -4 \times 10^{-4}. \quad (3.2)$$

From Fig. 2, one can see that it is possible that LISA (DECIGO) would be able to measure $\delta w(T)$ at this accuracy for phase-transition temperatures between $\sim 10^{4-6}$ GeV ($\sim 10^{4-10}$ GeV). As a result, both low scale and high scale SUSY can be tested at GW detectors. Because $w(T)$ is being measured at such a large temperature, as long as supersymmetry is present at temperatures below 10^{4-6} GeV, LISA could be able to test it.

Aside from supersymmetry, other models such as Twin Higgs [75] and Composite Higgs [76] also introduce a large number of degrees of freedom and predict deviations at the 10^{-3} level or larger. Meanwhile, models where the SM is UV completed into a conformal sector give a striking signature. Conformal sectors have $T_\mu^\mu = 0$ and thus predict $\delta w = 0$, unlike the SM prediction. As a result, we see that testing δw at the level of 10^{-3} probes almost all solutions to the electroweak hierarchy problem.

Almost all solutions to the hierarchy problem point to new physics at the TeV scale, while LISA tests if they are present below the 10^6 GeV scale. As a result, LISA has the potential to make a conclusive statement about our understanding of naturalness. DECIGO would be able to push these statements to the extreme and reach even the 10^{10} GeV scale.

3.2 $\sigma_w \lesssim 10^{-5}$

Another benchmark for a measurement of δw is 10^{-5} . At this level, one can test even the addition of a single degree of freedom to the SM bath at high temperatures, even if it is not free-streaming. There are many reasons to expect at least a single new particle in thermal equilibrium with the SM, a primary one being dark matter related. One of the simplest ways of producing dark matter is the process of thermal freeze-out. The fact that TeV scale weakly interacting particles undergoing the process of freeze-out gives the correct relic abundance is the famous “WIMP miracle”.

Dark matter models where the abundance is set through thermal freeze-out, in general require that the dark matter’s mass must be below 100 TeV. This is because if it were any heavier, then the cross section needed to reproduce the observed dark matter density would violate the unitarity bound. As such, most dark matter model which involves thermal freeze-out would be tested by a $\sigma_w \lesssim 10^{-5}$ measurement. The possibility of testing the most motivated mechanism of producing dark matter, rather than testing any model specifically, is what makes this limit appealing.

Another motivation for expecting at least a single new particle in thermal equilibrium is the axion. Axions are ubiquitous in UV complete models such as string theory and can solve problems such as the strong CP problem as well as be dark matter. For the sake of simplicity, we will focus on the axion coupling to photons, $g_{a\gamma\gamma}$. For a large range of parameters, the axion will be in thermal equilibrium with the SM after the GWs are generated. In this case, there will be a prediction of $\delta w \sim 10^{-5}$. The region of axion parameter space where this prediction is realized is shown in blue in Fig. 7.

3.3 $\sigma_{f_{FS}} \lesssim 10^{-2}$

The last benchmark value to explore is when $f_{FS} \sim 10^{-2}$. A free streaming fraction of 10^{-2} is present whenever there was a particle in thermal equilibrium that subsequently freezes out while still relativistic, much like what happens to the neutrinos. Aside from the fact that this exact process happened for neutrinos, there are other reasons to expect something similar could have happened in even earlier stages of the universe.

As in the previous example, one of the best motivated models that have free streaming particles is the axion. For large $g_{a\gamma\gamma}$, the axion was in thermal equilibrium giving $\delta w \sim 10^{-5}$. However for small $g_{a\gamma\gamma}$ the axion will have been in thermal equilibrium at early times and then have decoupled and become a free streaming particle in the sensitivity window of LISA/DECIGO. Thus a sensitivity to $f_{FS} \sim 10^{-2}$ would allow one to probe much of the parameter space of the axion, namely the region of parameter space shown in green in Fig. 7.

A final reason why a non-zero value of f_{FS} is motivated is that GWs themselves are free streaming particles. The current best bounds on GWs, independent of their frequency, comes from ΔN_{eff} constraints. A measurement of $f_{FS} \lesssim 10^{-2}$ is a sensitivity comparable to future constraints on GWs coming from CMB S4 experiments. Thus as long as LISA/DECIGO achieve a constraint better than this, they would be the strongest bound on new free streaming particles. A generic value to expect for f_{FS} due to GWs themselves can be seen using the total energy in GWs due to sound waves. This energy normalized to the total energy at the time of the phase transition is given by Ref. [65]

$$f_{FS} \geq \frac{\Omega_{GW}}{\Omega_{\text{total}}} \approx 5 \times 10^{-4} \left(\frac{100 H_{PT}}{\beta} \right) \left(\frac{4\alpha^2}{(1+\alpha)^2} \right), \quad (3.3)$$

where we are taking the bubble wall velocity to be 1 and 100% conversion of the vacuum energy into kinetic energy. In most models, $\alpha \sim 1$ but $\beta/H_{PT} \sim 100$, though some models can obtain smaller values of β . As a result, a reasonable value of the free streaming fraction to expect due to gravitational waves is $f_{FS} \gtrsim 10^{-3}$. Thus it is quite reasonable to expect that GWs themselves might be loud enough to comprise an observable value of f_{FS} . The example given above is simply one source of GWs. Different GW sources have different natural expectations for the value of f_{FS} .

4 Massive free streaming particles

The presence of relativistic free streaming particles affects the propagation of gravitational waves, since the energy momentum tensor of such particles develops an anisotropic stress in the presence of gravitational waves [38, 64]. In this section, we generalize this result by considering what happens when free streaming particles have a mass in order to study the impact of free streaming particles transitioning from being relativistic to non-relativistic. For the CMB, the fact that neutrinos are becoming non-relativistic around the time when the CMB is being generated leads to important imprints. For stochastic GWs, we find that as

free streaming particles become non-relativistic, their damping effect on the GW spectrum vanishes. The more e-foldings that the free streaming particles are relativistic after GW generation, the more they dampen the GWs.

4.1 Derivation of the damping

We start with the metric for tensor perturbations in an isotropic background, which is given by

$$\begin{aligned} g_{\mu\nu} &= a^2(t)(\delta_{\mu\nu} + h_{\mu\nu}(\vec{x}, t)), \\ h_{0\nu} &= 0, \end{aligned} \quad (4.1)$$

where $a(\tau)$ is the scale factor and $h_{\mu\nu}$ is a perturbation of the metric. We make a standard choice of transverse-traceless gauge (TT), meaning that $h_{ij,j} = 0$ and $h_i^i = 0$. The evolution of the remaining components of h_{ij} is governed by the linearized Einstein equation

$$-\frac{1}{2}h_{ij;\nu}^{\nu} = 8\pi G\Pi_{ij}, \quad (4.2)$$

where Π_{ij} is the anisotropic part of the energy-momentum tensor $T_{ij} = pg_{ij} + a^2\Pi_{ij}$. Knowing the form of the metric, defined in Eq. (4.1), we can unwrap covariant derivatives leading to the well-known equation

$$h''_{\lambda,k}(\tau) + 2\frac{a'}{a}h'_{\lambda,k}(\tau) + k^2h_{\lambda,k}(\tau) = 16\pi Ga^2\Pi_{\lambda,k}. \quad (4.3)$$

Here, the metric perturbations, h_{ij} , and anisotropic energy-momentum tensor, Π_{ij} , have been written in the momentum k and polarization λ space as

$$h_{ij}(\tau, x) = \sum_{\lambda=+,\times} \int \frac{d^3k}{(2\pi)^3} h_{\lambda,k}(\tau) e^{ikx} \epsilon_{ij}^{\lambda}, \quad (4.4)$$

$$\Pi_{ij}(\tau, x) = \sum_{\lambda=+,\times} \int \frac{d^3k}{(2\pi)^3} \Pi_{\lambda,k}(\tau) e^{ikx} \epsilon_{ij}^{\lambda}, \quad (4.5)$$

where $\epsilon_{ij}^{+,\times}$ are the polarization tensors. Our aim now is to determine the form of $\Pi_{\lambda,k}$ to linear order in the perturbations. The energy-momentum tensor is given by

$$T_{ij} = \frac{1}{\sqrt{-\det g}} \int d^3P F(\vec{x}, \tau, P_i) \frac{P_i P_j}{P^0} \quad (4.6)$$

where $F(x^i, \tau, P_i)$ is the phase space density and $P^\mu \equiv \frac{dx^\mu}{d\lambda}$. Switching to comoving momentum, q^μ , defined by

$$P_i = \left(\delta_{ik} + \frac{h_{ik}}{2} \right) q_k, \quad (4.7)$$

with $q_i = q\gamma_i$, where γ_i are the directional cosines, and doing a perturbative expansion for the phase-space distribution $F(\vec{x}, \tau, q, \vec{\gamma}) = F_0(\tau, q) + F_1(\vec{x}, \tau, q, \vec{\gamma}) + \dots$, one finds at first order

$$\Pi_{ij} = a^{-4}(\tau) \int d^3q F_1(\vec{x}, \tau, q, \gamma_i) \frac{q^2 \gamma_i \gamma_j}{\sqrt{q^2 + a^2 m^2}}. \quad (4.8)$$

For simplicity, we will assume that free streaming particles were once in thermal equilibrium and at some point decoupled from the rest of the bath. While this assumption is not necessary, it is the case for many motivated examples of free streaming particles. When a given particle species is in thermal equilibrium, its 0th order phase-space density is given by the thermal distribution in a homogeneous background

$$F(\vec{x}, \tau, q, \vec{\gamma}) = \frac{N}{(2\pi)^3} \left[\exp\left(\frac{\sqrt{q^2 + m^2 a(\tau)^2}}{a(\tau) k T}\right) \pm 1 \right]^{-1}, \quad (4.9)$$

where N is the number of degrees of freedom in that species. Assuming that a given species χ decouples at $\tau = \tau_d$, the evolution of the phase space density freezes

$$F_0(\tau > \tau_d, q) = \frac{N}{(2\pi)^3} \left[\exp\left(\frac{\sqrt{q^2 + m^2 a(\tau_d)^2}}{a(\tau_d) k T_d}\right) \pm 1 \right]^{-1} \approx \frac{N}{(2\pi)^3} \left[\exp\left(\frac{q}{a(\tau_d) k T_d}\right) \pm 1 \right]^{-1} \quad (4.10)$$

where we assume that χ decouples when $T_d \gg m$.

We can compute the evolution of the perturbation $F_1(\vec{x}, \tau, q^0, \vec{\gamma})$ by expanding the Boltzmann equation

$$\frac{dF}{d\tau} = \frac{\partial F}{\partial \tau} + \frac{dx^i}{d\tau} \frac{\partial F}{\partial x^i} + \frac{dq}{d\tau} \frac{\partial F}{\partial q} + \frac{d\gamma^i}{d\tau} \frac{\partial F}{\partial \gamma^i} = 0. \quad (4.11)$$

To leading order in h , the Boltzmann equation simplifies to

$$\frac{\partial F_1}{\partial \tau} + \gamma_i v \frac{\partial F_1}{\partial x^i} = \frac{1}{2} h'_{ij} \gamma_i \gamma_j q \frac{\partial F_0}{\partial q}, \quad (4.12)$$

where $v = q/\sqrt{q^2 + a^2 m^2}$. Going to Fourier space and using the polarization vectors we can decompose the perturbation F_1 into

$$F_1(\vec{x}, \tau, q, \vec{\gamma}) = \sum_{\lambda=+, \times} \int \frac{d^3k}{(2\pi)^3} e^{i\vec{k}\cdot\vec{x}} f_{k,\lambda}(\tau, \mu, q) \epsilon_{ij}^\lambda \gamma_i \gamma_j, \quad (4.13)$$

where $\mu = \hat{k} \cdot \vec{\gamma}$, leading to

$$\frac{\partial f_{k,\lambda}}{\partial \tau} + i v k \mu f_{k,\lambda} = q \frac{\partial F_0}{\partial q} \frac{1}{2} \frac{\partial h_{\lambda,k}}{\partial \tau}. \quad (4.14)$$

Assuming that there were no tensor perturbations in the free streaming radiation before the

gravitational waves were generated, we have

$$f_{k,\lambda}(\tau, q, \mu) = \frac{1}{2}q \frac{\partial F_0}{\partial q} \int_{\tau_{PT}}^{\tau} d\tau' h'(\tau') e^{-i \int_{\tau'}^{\tau} d\tau'' v(\tau'') k\mu}. \quad (4.15)$$

Plugging the above result into Eq. 4.8, one finds after some algebra

$$\Pi_{\lambda,k} = a^{-4} \int dq \frac{q^5}{\sqrt{q^2 + a^2 m^2}} \frac{\partial F_0}{\partial q} \int_{\tau_d}^{\tau} d\tau' h'(\tau') 4\pi \frac{j_2(u_q(\tau') - u_q(\tau))}{(u_q(\tau') - u_q(\tau))^2}, \quad (4.16)$$

where j_2 is the spherical Bessel function, and with u_q defined by

$$u_q(\tau) = k \int_{\tau_{PT}}^{\tau} d\tau' v(\tau'). \quad (4.17)$$

Combining results from Eq. (4.3) and Eq. (4.16) we get the general equation for how massive free streaming particles affect gravitational waves:

$$h''_{\lambda,k}(\tau) + 2\frac{a'}{a} h'_{\lambda,k}(\tau) + k^2 h_{\lambda,k}(\tau) = \frac{24\pi f_{FS}(\tau)}{\rho_{FS}(\tau)} \left(\frac{a'}{a}\right)^2 \int \frac{dq}{a^4} \frac{q^5}{\sqrt{q^2 + a^2 m^2}} \frac{\partial F_0}{\partial q} \times \int_{\tau_d}^{\tau} d\tau' h'(\tau') \frac{j_2(u_q(\tau') - u_q(\tau))}{(u_q(\tau') - u_q(\tau))^2}, \quad (4.18)$$

where ρ_{FS} is the average energy density in free streaming particles and $f_{FS}(\tau)$ is the free streaming fraction, Eq. 2.2. Note that in the massless limit, $u_q(\tau) = k\tau$, from which follows that in a radiation dominated universe Eq. (4.18) reduces to the previously known expression [38, 64]

$$h''_{\lambda,k}(\tau) + 2\frac{a'}{a} h'_{\lambda,k}(\tau) + k^2 h_{\lambda,k}(\tau) = -24f_{FS} \left(\frac{a'}{a}\right)^2 \int_{\tau_d}^{\tau} d\tau' h'(\tau') \frac{j_2(k(\tau' - \tau))}{(k(\tau' - \tau))^2}. \quad (4.19)$$

4.2 Numerical results

In this subsection, we present numerical solutions to the integro-differential equation 4.18 for different values of the free streaming particle's mass. Massive free streaming particles modify the gravitational wave spectrum via two effects, by changing the equation of state of the universe when they become non-relativistic, and by causing a suppression due to their free streaming nature. When the free streaming particles transition from being relativistic to non-relativistic, the change in the equation of state can drastically affect the expansion history (e.g., if these free streaming particles were stable and didn't annihilate they could lead to a period of early matter domination).

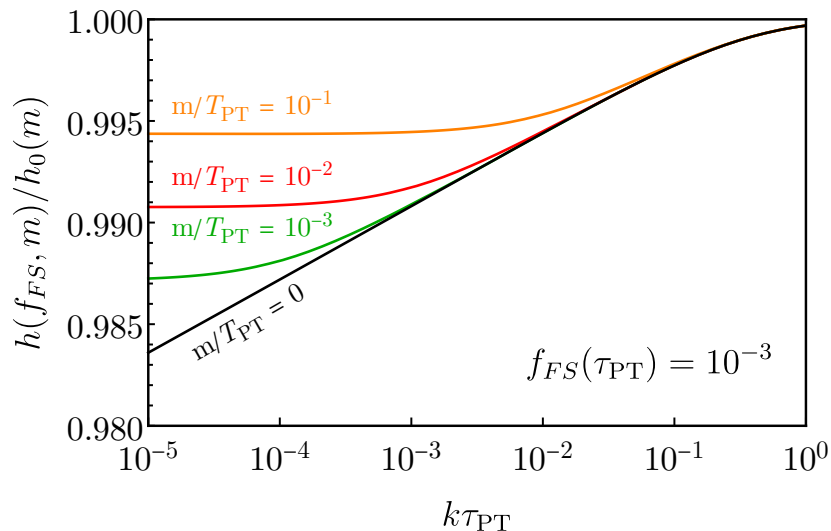


Figure 8. The fractional suppression of GWs due to massive free streaming particles as compared to massive interacting particles. We fix the free streaming fraction to be $f_{FS}(\tau_{PT}) = 10^{-3}$ and let the mass vary $m/T_{PT} = 10^{-1}, 10^{-2}, 10^{-3}, 0$, shown in orange, red, green and black respectively. When the free streaming particles becomes non-relativistic, they cease to suppress the gravitational waves leaving only the suppression that resulted from back when they were relativistic.

In order to isolate the effects on the GW spectrum due to particles free streaming from the ones coming from changes in the expansion history, we will compare ratios of the GW spectrum between two scenarios with the same expansion history. We include a new species that starts off relativistic and later transitions to the non-relativistic regime. In the first case this component is free streaming, $h(f_{FS}, m)$, while in the second case it is not, $h_0(m)$. In Fig. 8, we show the suppression $h(f_{FS}, m)/h_0(m)$ taking $f_{FS}(\tau_{PT}) = 10^{-3}$ for several masses $m/T_{PT} = 10^{-1}, 10^{-2}, 10^{-3}, 0$ in orange, red, green and black respectively.

In the massless case, the suppression is larger for smaller frequencies, causing a change in the shape of the GW spectrum as explored in the previous sections. For the massive case, at high frequencies that enter the horizon while the free streaming particles are relativistic, the suppression tracks the massless case. For low frequencies that enter the horizon after the free streaming particles are non-relativistic, the suppression asymptotes to a constant value at low frequencies. For the low frequency part of the spectrum, the majority of the suppression is from when the modes were super horizon and slow rolling in the potential generated by the relativistic free streaming particles, as discussed in Ref. [38].

5 Conclusion

In this article, we have demonstrated that LISA (DECIGO) can potentially measure the equation of state of the universe (w) and/or the fraction of free streaming particles (f_{FS}) down to an accuracy of 10^{-4} (10^{-6}). This measurement is analogous to 21-cm measurements

in that a deformation to a known frequency distribution is used to infer propagation effects. To illustrate the physics potential of such a precise measurement, we presented several benchmark models that predict deviations from an equation of state of $1/3$ at varying levels. The Standard Model itself predicts a $w - 1/3 \sim 10^{-3}$ deviation, well motivated solutions to the electroweak hierarchy problem predict different $w - 1/3 \gtrsim 10^{-3}$ deviations and dark matter models predict $w - 1/3 \sim 10^{-5}$. Many of these same models also predict a large $f_{FS} \sim 10^{-2}$. If LISA were to see stochastic GWs and were able to make this precision measurement, it would revolutionize our understanding of early universe physics.

The possibility of reaching these exciting benchmark values at LISA pushes for an understanding of all signals and noises at the 10^{-4} level, including contamination from astrophysical foregrounds, which would likely be significant for mid-band detectors like DECIGO. In this article, we assumed that the GW signal was generated in a short sub-horizon timescale and thus the shape of the frequency spectrum is fixed, e.g. sound waves can be sub-horizon [77] or super-horizon [78]. It is possible that some of the source of GWs may persist for longer than a Hubble time and thus contaminate the precise measurement of the equation of state. Our results thus motivate an improved understanding of all sources of GWs and their low frequency behavior. For example in a radiation dominated universe, $\Omega_{GW} \propto k^3 P_{GW}(k)$ with $P_{GW}(k)$ being the Fourier transform of the two point function of the source of GWs. For a causal source, there exists a radius R such that $P_{GW}(x > R) = 0$ implying that $P_{GW}(k \ll 1/R) \sim c_0 + c_1 k^2 R^2$ for some constants c_0 and c_1 . There is thus necessarily a model dependent k^5 correction to the k^3 scaling that needs to be accounted for.

If LISA were to discover stochastic GWs, GW physics could instantly become a precision science. It is exciting to see that in this case, that LISA would be able to teach us about the early universe to an unprecedented precision.

Acknowledgement

The authors were supported in part by the NSF grants PHY-1914480, PHY-1914731, by the Maryland Center for Fundamental Physics (MCFP). GMT was also partly funded by the US-Israeli BSF Grant 201823. GMT thanks the Aspen Center where part of this work was completed, which is supported by National Science Foundation grant PHY-1607611. The participation of GMT at the Aspen Center for Physics was supported by the Simons Foundation.

A Calculation of $w(T)$

In this section, we show how one calculates $\delta w(T) = w(T) - 1/3$ in various theories. For the sake of simplicity, we will work in the limit where all particles are massless. Our starting point is the first law of thermodynamics $dU = TdS - pdV$. We can express the total energy (entropy) in terms of the energy (entropy) density using $U = \rho(T)V$ ($S = s(T)V$). Equating

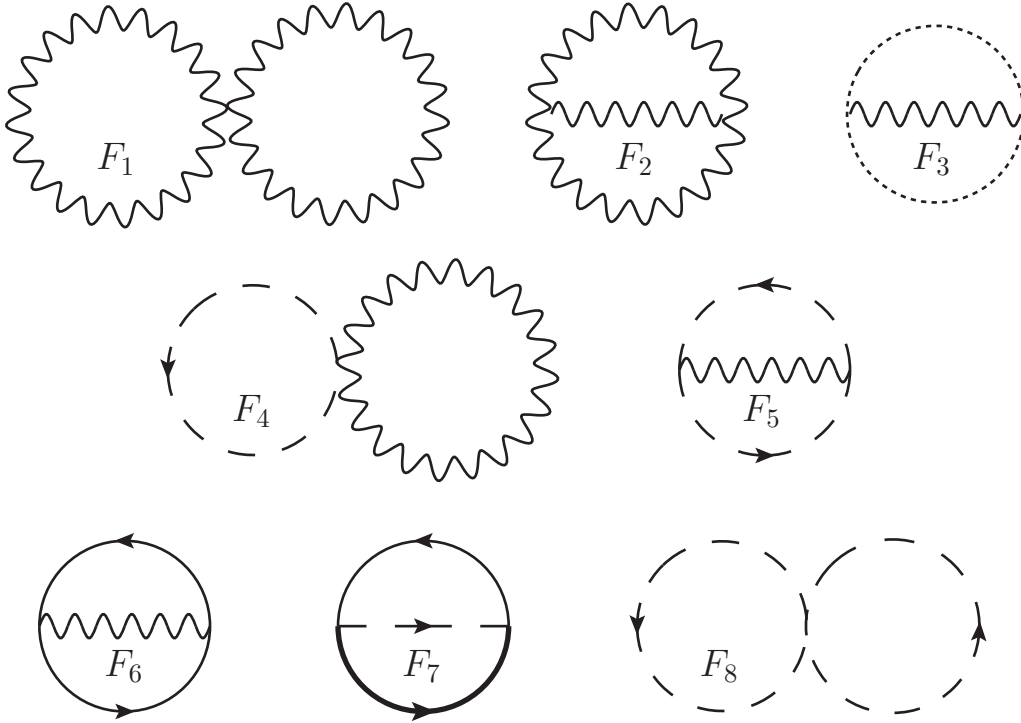


Figure 9. The eight leading order diagrams contributing to the free energy that lead to $w(T) \neq 1/3$. $F_{1,2,3}$ involve gauge bosons and/or ghosts and are present for any non-abelian gauge theory. $F_{4,5}$ (F_6) are present whenever there is a scalar (fermion) charged under a gauge group. F_7 is the leading diagram for Yukawa couplings while F_8 is the leading diagram for quartic couplings.

the dT and dV terms on both sides of the first law of thermodynamics, we arrive at

$$s = \frac{\rho + p}{T} \quad \rho = T \frac{dp}{dT} - p. \quad (\text{A.1})$$

Pressure can be exchanged with the free energy density using $f = \rho - Ts = -p$. After a bit of algebra, we find

$$\delta w(T) = \frac{T^4}{3\rho} \frac{d(f/T^4)}{d \log T}. \quad (\text{A.2})$$

Expressing the free energy as a Taylor series in terms of coupling constants, we see that the right hand side is proportional to beta functions and inversely proportional to g_* . Connected vacuum diagrams give the log of the partition function, and hence up to a minus sign give the free energy density ($F = -T \log Z$). The leading contribution to δw can thus be found by calculating all connected 2-loop vacuum diagrams and taking the appropriate derivatives.

The 2-loop vacuum diagrams that we are interested in are shown in Fig. 9. There are eight diagrams that can all be calculated and their high temperature/low mass results are

most easily expressed in terms of

$$I = \frac{T^2}{12} \quad \tilde{I} = -\frac{T^2}{24}. \quad (\text{A.3})$$

The first three diagrams are present in any non-Abelian gauge theory and evaluate to

$$F_1 = 3g^2 C_2(G) d(G) I^2 \quad F_2 = -\frac{9}{4} g^2 C_2(G) d(G) I^2 \quad F_3 = \frac{1}{4} g^2 C_2(G) d(G) I^2, \quad (\text{A.4})$$

where $d(G)$ is the dimension of the group and $C_2(G)$ is its quadratic casmir. The next two diagrams are present in any gauge theory with charged scalars

$$F_4 = 4g^2 C_2(R) d(R) I^2 \quad F_5 = -\frac{3}{2} g^2 C_2(R) d(R) I^2, \quad (\text{A.5})$$

where as before $d(R)$ ($C_2(R)$) is the dimension (quadratic casmir) of the representation. For abelian theories $C_2(R) = Q^2$. Diagram F_6 is present for theories with charged Weyl fermions and evaluates to

$$F_6 = g^2 C_2(R) d(R) (\tilde{I}^2 - 2\tilde{I}I). \quad (\text{A.6})$$

If there are Yukawa couplings involving a complex scalar Φ and two Weyl fermions ψ and ψ^c of the form $\mathcal{L} = y\Phi\psi\psi^c$, diagram F_7 will be present

$$F_7 = y^2 (\tilde{I}^2 - 2\tilde{I}I). \quad (\text{A.7})$$

Finally if there are scalar quartic couplings, then F_8 will be present. For a quartic coupling of the form, $\mathcal{L} = \lambda(H_i H_i^\dagger)^2$, we have

$$F_8 = \lambda N_H (1 + N_H) I^2 \quad (\text{A.8})$$

where N_H is the number of scalars that the index i runs over. For a different quartic coupling, e.g. those present in SUSY, the combinatorics factor, $N_H(1 + N_H)$, will be different.

We can now use the previous results to find the free energy density ($f = \sum F_i$) and combine it with Eq. A.2 and beta functions to find δw for various theories and at various temperatures.

The Standard Model : When calculating δw in the SM, we only take y_t, λ, g, g' and g_s to be non-zero and ignore all other couplings. The dominant contribution to δw comes from the QCD beta function because of both the abundance of colored particles and the size of the beta function. The top Yukawa beta function is the next most important contribution and contributes only about 5% of the final result. More explicitly, we find that at leading order

$$\delta w = \frac{T^4}{\rho} \left(\frac{55}{1728} \beta_{g'^2} + \frac{43}{576} \beta_{g^2} + \frac{7}{36} \beta_{g_s^2} + \frac{5}{288} \beta_{y_t^2} + \frac{1}{72} \beta_\lambda \right), \quad (\text{A.9})$$

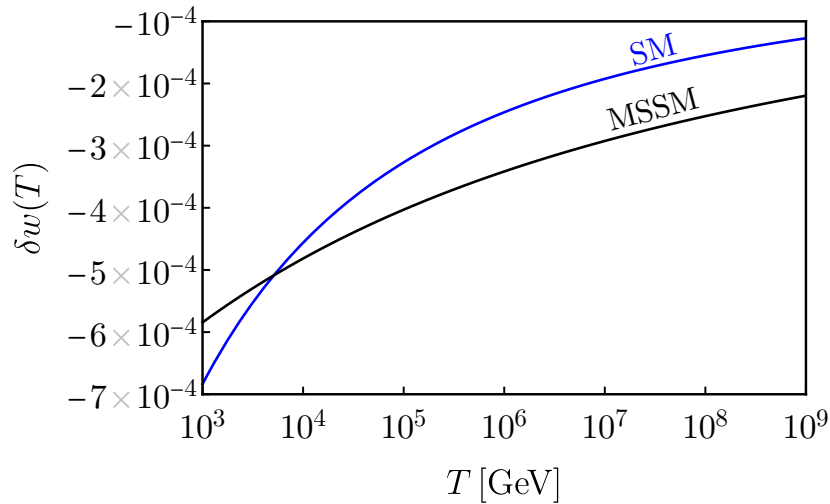


Figure 10. The deviation of equation of state from $1/3$ of the Standard Model (black) and the MSSM (blue) as a function of temperature.

where β are the beta functions defined as $\beta_\lambda = d\lambda/d\log\mu$. The value of $\delta w(T)$ for the SM is shown as the black line in Fig. 10.

The Minimal Supersymmetric Standard Model : The MSSM contains many more particles and interactions, but its QCD beta function is smaller than the SM value. As a result of these effects partially canceling, the MSSM value of δw is not very different from the SM value.

Because the Higgs quartic coupling is determined by gauge couplings, we only consider contributions from y_t, g, g' and g_s . As with the SM, the dominant contribution again comes from the QCD beta function with all other couplings playing an even smaller role than before. We find that at leading order

$$\delta w = \frac{T^4}{\rho} \left(\frac{33}{64}\beta_{g'^2} + \frac{69}{64}\beta_{g^2} + \frac{21}{8}\beta_{g_s^2} + \frac{9}{32}\beta_{y_t^2} \right). \quad (\text{A.10})$$

The value of $\delta w(T)$ for the MSSM is shown as the blue line in Fig. 10.

The Standard Model with doublet dark matter : The next model we consider is dark matter as a vector-like fermion with the quantum numbers of the Higgs boson. This is a particularly appealing version of WIMP dark matter as it makes the SM gauge couplings unify better [79]. Direct detection constraints imply that this WIMP necessarily mixes with an additional singlet, but this singlet can be much heavier than the WIMP and thus we will neglect it. As before, we only consider the couplings y_t, λ, g, g' and g_s . As the doublet is not

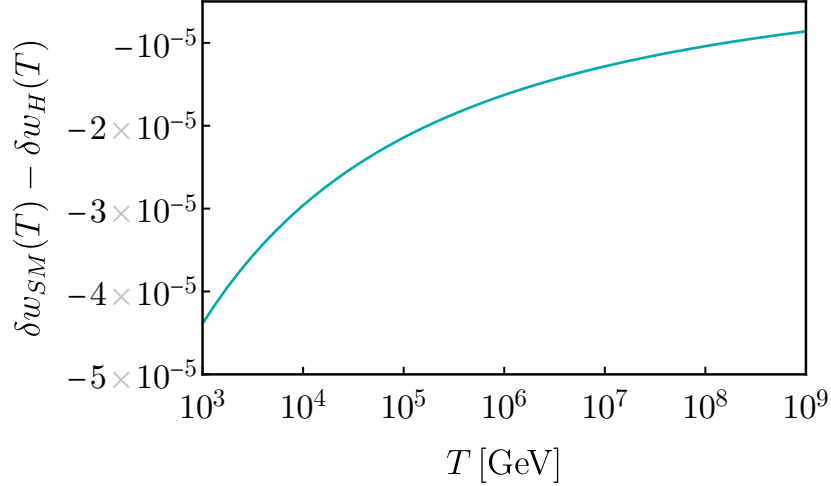


Figure 11. The difference in the equation of state of the Standard Model with and without a vector-like doublet dark matter.

color charged, it does not change the result by much. We find that

$$\delta w = \frac{T^4}{\rho} \left(\frac{5}{144} \beta_{g'^2} + \frac{1}{12} \beta_{g^2} + \frac{7}{36} \beta_{g_s^2} + \frac{5}{288} \beta_{y_i^2} + \frac{1}{72} \beta_\lambda \right). \quad (\text{A.11})$$

The difference between this result and the SM is shown in Fig. 11.

References

- [1] **LIGO Scientific, Virgo** Collaboration, B. P. Abbott et al., *Observation of Gravitational Waves from a Binary Black Hole Merger*, *Phys. Rev. Lett.* **116** (2016), no. 6 061102, [[arXiv:1602.03837](#)].
- [2] **LISA** Collaboration, P. Amaro-Seoane et al., *Laser Interferometer Space Antenna*, [[arXiv:1702.00786](#)].
- [3] G. M. Harry, P. Fritschel, D. A. Shaddock, W. Folkner, and E. S. Phinney, *Laser interferometry for the big bang observer*, *Class. Quant. Grav.* **23** (2006) 4887–4894. [Erratum: *Class.Quant.Grav.* 23, 7361 (2006)].
- [4] **MAGIS** Collaboration, P. W. Graham, J. M. Hogan, M. A. Kasevich, S. Rajendran, and R. W. Romani, *Mid-band gravitational wave detection with precision atomic sensors*, [[arXiv:1711.02225](#)].
- [5] S. Kawamura et al., *The Japanese space gravitational wave antenna: DECIGO*, *Class. Quant. Grav.* **28** (2011) 094011.
- [6] L. Grishchuk, *Amplification of gravitational waves in an isotropic universe*, *Sov. Phys. JETP* **40** (1975) 409–415.
- [7] A. A. Starobinsky, *Spectrum of relict gravitational radiation and the early state of the universe*, *JETP Lett.* **30** (1979) 682–685.

- [8] V. Rubakov, M. Sazhin, and A. Veryaskin, *Graviton Creation in the Inflationary Universe and the Grand Unification Scale*, *Phys. Lett. B* **115** (1982) 189–192.
- [9] M. Guzzetti, N. Bartolo, M. Liguori, and S. Matarrese, *Gravitational waves from inflation*, *Riv. Nuovo Cim.* **39** (2016), no. 9 399–495, [[arXiv:1605.01615](#)].
- [10] S. Khlebnikov and I. Tkachev, *Relic gravitational waves produced after preheating*, *Phys. Rev. D* **56** (1997) 653–660, [[hep-ph/9701423](#)].
- [11] R. Easther and E. A. Lim, *Stochastic gravitational wave production after inflation*, *JCAP* **04** (2006) 010, [[astro-ph/0601617](#)].
- [12] R. Easther, J. Giblin, John T., and E. A. Lim, *Gravitational Wave Production At The End Of Inflation*, *Phys. Rev. Lett.* **99** (2007) 221301, [[astro-ph/0612294](#)].
- [13] J. Garcia-Bellido and D. G. Figueroa, *A stochastic background of gravitational waves from hybrid preheating*, *Phys. Rev. Lett.* **98** (2007) 061302, [[astro-ph/0701014](#)].
- [14] J. Garcia-Bellido, D. G. Figueroa, and A. Sastre, *A Gravitational Wave Background from Reheating after Hybrid Inflation*, *Phys. Rev. D* **77** (2008) 043517, [[arXiv:0707.0839](#)].
- [15] J. F. Dufaux, A. Bergman, G. N. Felder, L. Kofman, and J.-P. Uzan, *Theory and Numerics of Gravitational Waves from Preheating after Inflation*, *Phys. Rev. D* **76** (2007) 123517, [[arXiv:0707.0875](#)].
- [16] C. Caprini et al., *Detecting gravitational waves from cosmological phase transitions with LISA: an update*, *JCAP* **03** (2020) 024, [[arXiv:1910.13125](#)].
- [17] C. Caprini and D. G. Figueroa, *Cosmological Backgrounds of Gravitational Waves*, *Class. Quant. Grav.* **35** (2018), no. 16 163001, [[arXiv:1801.04268](#)].
- [18] N. Christensen, *Stochastic Gravitational Wave Backgrounds*, *Rept. Prog. Phys.* **82** (2019), no. 1 016903, [[arXiv:1811.08797](#)].
- [19] V. Acquaviva, N. Bartolo, S. Matarrese, and A. Riotto, *Second order cosmological perturbations from inflation*, *Nucl. Phys. B* **667** (2003) 119–148, [[astro-ph/0209156](#)].
- [20] S. Mollerach, D. Harari, and S. Matarrese, *CMB polarization from secondary vector and tensor modes*, *Phys. Rev. D* **69** (2004) 063002, [[astro-ph/0310711](#)].
- [21] D. Baumann, P. J. Steinhardt, K. Takahashi, and K. Ichiki, *Gravitational Wave Spectrum Induced by Primordial Scalar Perturbations*, *Phys. Rev. D* **76** (2007) 084019, [[hep-th/0703290](#)].
- [22] J. R. Espinosa, D. Racco, and A. Riotto, *A Cosmological Signature of the SM Higgs Instability: Gravitational Waves*, *JCAP* **1809** (2018), no. 09 012, [[arXiv:1804.07732](#)].
- [23] K. Kohri and T. Terada, *Semianalytic calculation of gravitational wave spectrum nonlinearly induced from primordial curvature perturbations*, *Phys. Rev. D* **97** (2018), no. 12 123532, [[arXiv:1804.08577](#)].
- [24] G. Domènech, *Induced gravitational waves in a general cosmological background*, *Int. J. Mod. Phys. D* **29** (2020), no. 03 2050028, [[arXiv:1912.05583](#)].
- [25] M. B. Hindmarsh, M. Lüben, J. Lumma, and M. Pauly, *Phase transitions in the early universe*, *SciPost Phys. Lect. Notes* **24** (2021) 1, [[arXiv:2008.09136](#)].

- [26] D. I. Dunsky, A. Ghoshal, H. Murayama, Y. Sakakihara, and G. White, *Gravitational Wave Astronomy*, [arXiv:2111.08750](#).
- [27] C. Grojean and G. Servant, *Gravitational Waves from Phase Transitions at the Electroweak Scale and Beyond*, *Phys. Rev. D* **75** (2007) 043507, [[hep-ph/0607107](#)].
- [28] P. Schwaller, *Gravitational Waves from a Dark Phase Transition*, *Phys. Rev. Lett.* **115** (2015), no. 18 181101, [[arXiv:1504.07263](#)].
- [29] C.-F. Chang and Y. Cui, *Stochastic Gravitational Wave Background from Global Cosmic Strings*, *Phys. Dark Univ.* **29** (2020) 100604, [[arXiv:1910.04781](#)].
- [30] Y. Gouttenoire, G. Servant, and P. Simakachorn, *BSM with Cosmic Strings: Heavy, up to EeV mass, Unstable Particles*, *JCAP* **07** (2020) 016, [[arXiv:1912.03245](#)].
- [31] Y. Cui, M. Lewicki, and D. E. Morrissey, *Gravitational Wave Bursts as Harbingers of Cosmic Strings Diluted by Inflation*, *Phys. Rev. Lett.* **125** (2020), no. 21 211302, [[arXiv:1912.08832](#)].
- [32] W. Buchmuller, V. Domcke, H. Murayama, and K. Schmitz, *Probing the scale of grand unification with gravitational waves*, *Phys. Lett. B* **809** (2020) 135764, [[arXiv:1912.03695](#)].
- [33] J. A. Dror, T. Hiramatsu, K. Kohri, H. Murayama, and G. White, *Testing the Seesaw Mechanism and Leptogenesis with Gravitational Waves*, *Phys. Rev. Lett.* **124** (2020), no. 4 041804, [[arXiv:1908.03227](#)].
- [34] D. Dunsky, L. J. Hall, and K. Harigaya, *Dark Matter, Dark Radiation and Gravitational Waves from Mirror Higgs Parity*, *JHEP* **02** (2020) 078, [[arXiv:1908.02756](#)].
- [35] S. Blasi, V. Brdar, and K. Schmitz, *Fingerprint of low-scale leptogenesis in the primordial gravitational-wave spectrum*, *Phys. Rev. Res.* **2** (2020), no. 4 043321, [[arXiv:2004.02889](#)].
- [36] C. S. Machado, W. Ratzinger, P. Schwaller, and B. A. Stefanek, *Gravitational wave probes of axionlike particles*, *Phys. Rev. D* **102** (2020), no. 7 075033, [[arXiv:1912.01007](#)].
- [37] M. Geller, A. Hook, R. Sundrum, and Y. Tsai, *Primordial Anisotropies in the Gravitational Wave Background from Cosmological Phase Transitions*, *Phys. Rev. Lett.* **121** (2018), no. 20 201303, [[arXiv:1803.10780](#)].
- [38] A. Hook, G. Marques-Tavares, and D. Racco, *Causal gravitational waves as a probe of free streaming particles and the expansion of the Universe*, *JHEP* **02** (2021) 117, [[arXiv:2010.03568](#)].
- [39] N. Seto and J. Yokoyama, *Probing the equation of state of the early universe with a space laser interferometer*, *J. Phys. Soc. Jap.* **72** (2003) 3082–3086, [[gr-qc/0305096](#)].
- [40] L. A. Boyle and P. J. Steinhardt, *Probing the early universe with inflationary gravitational waves*, *Phys. Rev. D* **77** (2008) 063504, [[astro-ph/0512014](#)].
- [41] Y. Watanabe and E. Komatsu, *Improved Calculation of the Primordial Gravitational Wave Spectrum in the Standard Model*, *Phys. Rev. D* **73** (2006) 123515, [[astro-ph/0604176](#)].
- [42] L. A. Boyle and A. Buonanno, *Relating gravitational wave constraints from primordial nucleosynthesis, pulsar timing, laser interferometers, and the CMB: Implications for the early Universe*, *Phys. Rev. D* **78** (2008) 043531, [[arXiv:0708.2279](#)].
- [43] R. Jinno, T. Moroi, and K. Nakayama, *Probing dark radiation with inflationary gravitational waves*, *Phys. Rev. D* **86** (2012) 123502, [[arXiv:1208.0184](#)].

- [44] C. Caprini et al., *Science with the space-based interferometer eLISA. II: Gravitational waves from cosmological phase transitions*, *JCAP* **04** (2016) 001, [[arXiv:1512.06239](#)].
- [45] K. Saikawa and S. Shirai, *Primordial gravitational waves, precisely: The role of thermodynamics in the Standard Model*, *JCAP* **05** (2018) 035, [[arXiv:1803.01038](#)].
- [46] Y. Cui, M. Lewicki, D. E. Morrissey, and J. D. Wells, *Probing the pre-BBN universe with gravitational waves from cosmic strings*, *JHEP* **01** (2019) 081, [[arXiv:1808.08968](#)].
- [47] R. R. Caldwell, T. L. Smith, and D. G. Walker, *Using a Primordial Gravitational Wave Background to Illuminate New Physics*, *Phys. Rev. D* **100** (2019), no. 4 043513, [[arXiv:1812.07577](#)].
- [48] F. D’Eramo and K. Schmitz, *Imprint of a scalar era on the primordial spectrum of gravitational waves*, *Phys. Rev. Research*. **1** (2019) 013010, [[arXiv:1904.07870](#)].
- [49] D. G. Figueroa and E. H. Tanin, *Ability of LIGO and LISA to probe the equation of state of the early Universe*, *JCAP* **1908** (2019) 011, [[arXiv:1905.11960](#)].
- [50] P. Auclair et al., *Probing the gravitational wave background from cosmic strings with LISA*, *JCAP* **04** (2020) 034, [[arXiv:1909.00819](#)].
- [51] Y. Gouttenoire, G. Servant, and P. Simakachorn, *Beyond the Standard Models with Cosmic Strings*, *JCAP* **07** (2020) 032, [[arXiv:1912.02569](#)].
- [52] G. Domènech, S. Pi, and M. Sasaki, *Induced gravitational waves as a probe of thermal history of the universe*, *JCAP* **08** (2020) 017, [[arXiv:2005.12314](#)].
- [53] R. Allahverdi et al., *The First Three Seconds: a Review of Possible Expansion Histories of the Early Universe*, [arXiv:2006.16182](#).
- [54] R.-G. Cai, S. Pi, and M. Sasaki, *Universal infrared scaling of gravitational wave background spectra*, [arXiv:1909.13728](#).
- [55] C. Caprini, R. Durrer, T. Konstandin, and G. Servant, *General Properties of the Gravitational Wave Spectrum from Phase Transitions*, *Phys. Rev.* **D79** (2009) 083519, [[arXiv:0901.1661](#)].
- [56] R. Sundrum, *Tasi 2004 lectures: To the fifth dimension and back*, in *Theoretical Advanced Study Institute in Elementary Particle Physics: Physics in $D \geq 4$* , pp. 585–630, 8, 2005. [hep-th/0508134](#).
- [57] C. Csáki, S. Lombardo, and O. Telem, *TASI Lectures on Non-supersymmetric BSM Models*, pp. 501–570. WSP, 2018. [arXiv:1811.04279](#).
- [58] T. Lin, *Dark matter models and direct detection*, *PoS* **333** (2019) 009, [[arXiv:1904.07915](#)].
- [59] K. Griest and M. Kamionkowski, *Unitarity Limits on the Mass and Radius of Dark Matter Particles*, *Phys. Rev. Lett.* **64** (1990) 615.
- [60] R. D. Peccei and H. R. Quinn, *CP Conservation in the Presence of Instantons*, *Phys. Rev. Lett.* **38** (1977) 1440–1443.
- [61] R. D. Peccei and H. R. Quinn, *Constraints Imposed by CP Conservation in the Presence of Instantons*, *Phys. Rev. D* **16** (1977) 1791–1797.
- [62] S. Weinberg, *A New Light Boson?*, *Phys. Rev. Lett.* **40** (1978) 223–226.

- [63] F. Wilczek, *Problem of Strong P and T Invariance in the Presence of Instantons*, *Phys. Rev. Lett.* **40** (1978) 279–282.
- [64] S. Weinberg, *Damping of tensor modes in cosmology*, *Phys. Rev. D* **69** (2004) 023503, [[astro-ph/0306304](#)].
- [65] M. Hindmarsh, S. J. Huber, K. Rummukainen, and D. J. Weir, *Shape of the acoustic gravitational wave power spectrum from a first order phase transition*, *Phys. Rev. D* **96** (2017), no. 10 103520, [[arXiv:1704.05871](#)]. [Erratum: *Phys.Rev.D* 101, 089902 (2020)].
- [66] J. Ellis, M. Lewicki, and J. M. No, *On the Maximal Strength of a First-Order Electroweak Phase Transition and its Gravitational Wave Signal*, *JCAP* **04** (2019) 003, [[arXiv:1809.08242](#)].
- [67] J. Ellis, M. Lewicki, and J. M. No, *Gravitational waves from first-order cosmological phase transitions: lifetime of the sound wave source*, *JCAP* **07** (2020) 050, [[arXiv:2003.07360](#)].
- [68] B. Allen and J. D. Romano, *Detecting a stochastic background of gravitational radiation: Signal processing strategies and sensitivities*, *Phys. Rev. D* **59** (1999) 102001, [[gr-qc/9710117](#)].
- [69] M. Maggiore, *Gravitational wave experiments and early universe cosmology*, *Phys. Rept.* **331** (2000) 283–367, [[gr-qc/9909001](#)].
- [70] H. Kudoh, A. Taruya, T. Hiramatsu, and Y. Himemoto, *Detecting a gravitational-wave background with next-generation space interferometers*, *Phys. Rev. D* **73** (2006) 064006, [[gr-qc/0511145](#)].
- [71] C. Caprini, D. G. Figueroa, R. Flauger, G. Nardini, M. Peloso, M. Pieroni, A. Ricciardone, and G. Tasinato, *Reconstructing the spectral shape of a stochastic gravitational wave background with LISA*, *JCAP* **11** (2019) 017, [[arXiv:1906.09244](#)].
- [72] C. Gowling and M. Hindmarsh, *Observational prospects for phase transitions at LISA: Fisher matrix analysis*, *JCAP* **10** (2021) 039, [[arXiv:2106.05984](#)].
- [73] S. Kuroyanagi, T. Chiba, and N. Sugiyama, *Prospects for Direct Detection of Inflationary Gravitational Waves by Next Generation Interferometric Detectors*, *Phys. Rev. D* **83** (2011) 043514, [[arXiv:1010.5246](#)].
- [74] S. P. Martin, *A Supersymmetry primer*, *Adv. Ser. Direct. High Energy Phys.* **18** (1998) 1–98, [[hep-ph/9709356](#)].
- [75] Z. Chacko, H.-S. Goh, and R. Harnik, *The Twin Higgs: Natural electroweak breaking from mirror symmetry*, *Phys. Rev. Lett.* **96** (2006) 231802, [[hep-ph/0506256](#)].
- [76] R. Contino, *The Higgs as a Composite Nambu-Goldstone Boson*, in *Theoretical Advanced Study Institute in Elementary Particle Physics: Physics of the Large and the Small*, pp. 235–306, 2011. [arXiv:1005.4269](#).
- [77] J. Ellis, M. Lewicki, J. M. No, and V. Vaskonen, *Gravitational wave energy budget in strongly supercooled phase transitions*, *JCAP* **06** (2019) 024, [[arXiv:1903.09642](#)].
- [78] M. Hindmarsh, S. J. Huber, K. Rummukainen, and D. J. Weir, *Numerical simulations of acoustically generated gravitational waves at a first order phase transition*, *Phys. Rev. D* **92** (2015), no. 12 123009, [[arXiv:1504.03291](#)].
- [79] R. Mahbubani and L. Senatore, *The Minimal model for dark matter and unification*, *Phys. Rev. D* **73** (2006) 043510, [[hep-ph/0510064](#)].